Disclosing mechanical and specific structural characteristics of thick and adherent nanodiamond composite hard coating deposited on WC−Co substrates.

MURASAWA, K., DIAB, M.R, ATTA, H., NARAGINO, H., EL-SHAER, A., YOSHITAKE, T. and EGIZA, M.

2024

Materials Today Communications 40 (2024) 109839

Contents lists available at ScienceDirect

Materials Today Communications

journal homepage: www.elsevier.com/locate/mtcomm

Disclosing mechanical and specific structural characteristics of thick and adherent nanodiamond composite hard coating deposited on WC−Co substrates

Koki Murasawa [a,b], Mohamed R. Diab [a,d], Hoda Atta [c], Hiroshi Naragino [a], Abdelhamid El-Shaer [c], Tsuyoshi Yoshitake [a,*], Mohamed Egiza [d,e,**]

[a] Department of Advanced Energy Science and Engineering, Faculty of Engineering Sciences, Kyushu University, Kasuga, Fukuoka 816-8580, Japan
[b] OSG Corporation, 3-22 Honnogahara, Toyokawa, Aichi 442-8543, Japan
[c] Department of physics, Faculty of Science, KafrelSheikh University, Kafr El-Sheikh 33516, Egypt
[d] Department of Mechanical Engineering, Kafrelsheikh University, Kafrelsheikh 33516, Egypt
[e] School of Engineering, Robert Gordon University, Garthdee Road, Aberdeen AB10 7GJ, UK

ARTICLE INFO

Keywords:
Nanocomposite films
Hard coatings
WC−Co
DLC
Cathodic arc
Raman

ABSTRACT

Nanodiamond composite (NDC) films, with a notable hardness of 65 GPa and a substantial thickness of 10 μm, were successfully fabricated on unheated WC−Co substrates using cathodic arc plasma deposition (CAPD) technology. Raman and synchrotron-based structural analysis, comparing NDC films with similarly hard tetrahedral amorphous carbon (ta-C) films and chemical vapor deposition (CVD) diamond, unveiled distinctive features. Visible Raman spectroscopy highlighted NDC's unique nanostructured composition, characterized by nanodiamond grains embedded in an amorphous carbon matrix, resulting in a high fraction of C−C sp^3 bonds (70 %) and intense σ* C−C resonance contributing to its observed hardness. The small size of diamond crystals induced numerous grain boundaries, as evident through intense t-PA Raman peaks, effectively suppressing internal stress to 2.77 GPa and enabling the deposition of an impressive thickness (10 μm), surpassing the thinness of hard ta-C (< 1 μm). Despite the substantial thickness, NDC films demonstrated remarkable films-substrate adhesion, with no delamination and minimal spallation, in contrast to observed buckling and delamination in CVD diamond during Rockwell testing at various loads (60 Kg and 100 Kg). Additionally, NDC films maintained a stable and low coefficient of friction (≤ 0.1) against an Al_2O_3 counter-body, compared to the higher coefficient (≥ 0.25) of the bare WC-Co substrate. Furthermore, NDC deposition boasted a rapid rate (3.5 μm/h), significantly exceeding both ta-C and diamond coatings, enhancing its practical applicability. Significantly, the deposition process for NDC films stands out for its environmental friendliness and cost-effectiveness, involving no external heating, chemical reactions, chemical etching of Co, or nanodiamond seeding. The findings underscore the exceptional potential of NDC as a strong competitor to hard ta-C and CVD diamond coatings, especially in advanced cutting tool applications.

1. Introduction

Cobalt-cemented tungsten carbide (WC−Co) cutting tools are widely used for their high toughness but wear quickly when machining difficult-to-cut materials like carbon fibre-reinforced polymer (CFRP), titanium, silicon carbide, and aluminium-silicon alloys [1,2]. To address this challenge, hard coatings like diamond and diamond-like carbon (DLC) are applied, offering high hardness, wear resistance, smooth surfaces, cost-effectiveness, and extended tool lifetime [3–5]. Diamond coatings, deposited via chemical vapor deposition (CVD), provide exceptional hardness and wear resistance but have drawbacks like rough surfaces, low deposition rates, high cost, and chemical hazards particularly during substrate pretreatment [6,7]. Furthermore, hard DLC coatings known as tetrahedral amorphous carbon (ta-C), deposited via physical vapor deposition (PVD), offer high hardness and low coefficient of friction but have limited thickness and high internal stress affecting

* Corresponding author.
** Corresponding author at: Department of Mechanical Engineering, Kafrelsheikh University, Kafrelsheikh 33516, Egypt.
E-mail addresses: Tsuyoshi_yoshitake@kyudai.jp (T. Yoshitake), Mohamed_Egiza@eng.kfs.edu.eg (M. Egiza).

https://doi.org/10.1016/j.mtcomm.2024.109839
Received 2 May 2024; Received in revised form 9 July 2024; Accepted 14 July 2024
Available online 15 July 2024

adhesion and tool lifetime [5,8]. Among PVD methods, arc ion plating is a powerful technique widely used in the industry for the deposition of ta-C coatings, exhibiting high degrees of ionization and suitability for mass-production ability [9].

To meet hard coating demands and be environmentally friendly, an alternative PVD hard carbon coating is crucial for improving cutting performance. Nanodiamond composite (NDC) films deposited by cathodic arc plasma deposition (CAPD), a PVD method, exhibit interesting structural and mechanical properties, with numerous nanodiamond crystallites ($\leq$ 10 nm) embedded in an amorphous carbon (a-C) matrix [10,11]. This unique nanostructure composite can leverage the benefits of both diamond and DLC films while circumventing their limitations.

Preparation techniques significantly influence coating properties, impacting surface integrity, morphology, microstructure, stress state, interfacial structure, cohesion, and adhesion. Coatings with micro- or nano-scaled structures are customized using diverse techniques to meet specific performance requirements under varying working conditions [12]. CAPD successfully deposits NDC films using highly energetic carbon species ejected from a cylindrical anode towards the substrate surface [13]. The unique cylindrical anode structure facilitates a supersaturated condition with highly energetic ions, crucial for the formation of NDC films containing nanodiamond crystals in a rich C−C sp^3 a-C matrix. Previous research [14] demonstrated control over the size of these nanodiamond crystals (2.4–15.0 nm) by varying the arc discharge energy (1.8–144.0 J/pulse). These versatile films can be deposited on Si [15], SiC [16], Ti [17], and WC−Co substrates [18,19], finding applications in microelectromechanical systems, implants, and advanced cutting tools, with competitive properties.

The film's properties can be precisely controlled and tailored to meet specific application requirements by doping with Si [11], B [20], Cr [21] and adjusting preparation conditions like plasma energy [14,22], substrate temperature [23], and substrate biasing [24,25]. Importantly, unlike CVD diamond coatings, pretreatment of the Si and WC−Co substrate surface is not necessary [26,27]. NDC films grow directly on WC−Co without the need for chemical etching of Co from the substrate surface or/and seeding with nanodiamond. The Co diffusion into the NDC films is hardly occurred at room substrate-temperature or at 550 °C [23].

NDC films can be effectively evaluated using multiple techniques, including Nanoindentation, a well-established method, facilitates the measurement of hardness and Young's modulus [28]. Microscopic analysis, often performed using scanning electron microscopy (SEM), reveals surface morphology, while various spectroscopic techniques provide in-depth structural information. X-ray photoelectron spectroscopy (XPS), Near-Edge X-ray Absorption Fine Structure (NEXAFS), and Raman spectroscopy are commonly used tools, offering valuable insights into bonding configurations and material properties [19,29]. Notably, synchrotron radiation-based approaches enhance sensitivity and energy resolution, allowing for the exploration of a wider range of chemical states within the films.

For carbon-based materials like NDC films, visible Raman spectroscopy holds value due to its high sensitivity to carbon-carbon bonding and crystal structures. However, it's important to acknowledge that while this technique exhibits greater sensitivity to sp^2 bonded carbons when excited by visible light, it provides an indirect assessment of the sp^3 fraction within the films [30]. Additionally, Raman spectroscopy, along with X-ray diffraction (XRD) and the curvature method, can be employed for evaluating the internal stress state within the films [23,31].

The properties of carbon materials heavily depend on the ratio of C═C sp^2 (graphite-like) to C−C sp^3 (diamond-like) bonds. While diamond possesses predominantly C−C sp^3 bonds, DLC can exhibit a mix of sp^3, sp^2, and even sp^1 sites. The C−C sp^3 phase of diamond is crystalline, while in DLC, it is amorphous. The remaining C═C sp^2 fraction consists of amorphous carbon and olefinic molecules. The high fraction of C−C sp^3 bonds in a carbon film contributes to its hardness [26]. However, this increase in hardness is often associated with compressive stress [32], which can lead to film delamination and reduced adhesion strength. The high intrinsic compressive stress of ta-C films limits their practical applications, and various methods, such as incorporating doped elements [33], adhesion interlayers [34,35], thermal annealing, and multilayer structures [36], have been studied to reduce this stress. However, dopant impurities and annealing-induced graphitization can decrease film hardness and wear resistance. In high sp^3-content films, the stress prevents the growth of films as a single-layer with thickness $\geq$ 0.5 μm [8].

Beyond hardness and adhesion, achieving a low Coefficient of Friction (COF) is crucial for sustainable machining, especially under harsh conditions like high speeds, rough surfaces of counter body, heavy loads, and lack of lubrication. Therefore, the development of a new hard carbon material with low COF in harsh conditions, and high hardness comparable to diamond and ta-C, but with low compressive stress and thus thick film ($\geq$ 5 μm), is crucial to enhance films' adhesion and enable the growth of thick films. Such a material would offer improved coating properties and a wide range of practical applications.

In this work, NDC film was deposited by CAPD on WC−Co for advanced cutting tool applications. The film underwent a comprehensive analysis using nanoindentation, Rockwell indentation, SEM, XPS, NEXAFS, and Raman techniques, including the evaluation of its internal stress and COF in harsh conditions. These analyses were performed to investigate the specific structural characteristics of the NDC film in comparison to ta-C and CVD diamond films. The study aims to shed light on the factors contributing to the exceptional mechanical properties of NDC films, which exhibit comparable hardness to ta-C films combined with thickness like diamond films.

2. Experimental methods

2.1. Films preparation

This study utilized K-type cemented carbide (WC−Co) substrates with dimensions of φ10 × 5 mm for NDC film deposition. The WC−Co substrates possessed an intentionally rough surface, characterized by a roughness (Ra) ranging from 0.15 to 0.2 μm, to promote film adhesion. Additionally, a separate set of WC−Co samples (length: 20 mm, diameter: 6 mm, spherical end radius: 6 mm) were prepared for dedicated friction testing.

A coaxial arc plasma gun (model: ULVAC, APG-1000) equipped with a high-purity graphite rod (φ10 × 30 mm, 99.99 % C) served as the deposition source for the CAPD system. Prior to deposition, the arc plasma gun head was positioned at a distance of 10 mm from the WC−Co substrates. The deposition chamber was then evacuated to a base pressure below 10^{-4} Pa using a turbomolecular pump. During the CAPD process, the primary thermal influence on the WC−Co substrate originated from the generated plasma. The arc plasma gun operated with a voltage of 120 V, a capacitance of 720 μF, and a repetition rate of 1 Hz.

2.2. Films characterization

A suite of techniques assessed the films' mechanical properties, adhesion, and tribological behaviour. Nanoindentation using a Berkovich diamond tip determined hardness and Young's modulus. Prior to testing, films underwent mechanical polishing with silicon nanoparticles in olive oil to achieve a smooth surface (Ra $\leq$ 20 nm) minimizing roughness effects on measurements. Twenty indentations across the film surface ensured data consistency and accounted for potential inhomogeneity. The tests employed a maximum load of 5.0 mN, constant loading rate of 5.0 mN/s, and a 5-second hold at peak load. Film adhesion to WC-Co substrates was evaluated via Rockwell indentation with varying loads (60 kg and 100 kg).

Tribological performance was investigated using a pin-on-disk apparatus. All pin samples (NDC, ta-C, CVD diamond, and uncoated WC−Co) were tested in harsh conditions against rough alumina (Al_2O_3) counter-body (Ra= 355 nm) under dry, open-air conditions with a linear speed of 200 mm/s. NDC and CVD diamond films underwent a 60-minute test at 300 g load. In contrast, the uncoated WC−Co substrate and ta-C films were subjected to a shorter 10-minute test at the same 300 g load to assess their initial performance. Additionally, a separate test was conducted for ta-C films at a lower load of 25 g and a slower linear speed of 25 mm/s to investigate the influence of these parameters on its tribological behaviour.

To evaluate internal stress within the NDC film, a thin film (175 nm) was deposited on a thicker silicon (Si) substrate (260 μm, (100) orientation, 15 mm×5 mm). The bending curvature of the film was measured parallel to the Si [111] crystallographic direction along the long side (15 mm) using a surface profiler while the sample was fixed on one end only. This technique provided an indirect assessment of internal stress in the film. In contrast, the internal stress of the CVD diamond film was directly measured using XRD on the as-deposited 10 μm thick film.

Scanning electron microscopy (SEM) with a JEOL JSM-6500 F instrument was employed to examine the morphology, or surface features, of the NDC film. To understand the chemical bonding structure of the films and their influence on mechanical properties, X-ray photoelectron spectroscopy (XPS) and Near-Edge X-ray Absorption Fine Structure (NEXAFS) spectroscopy were utilized. XPS measurements were conducted on the as-deposited film surface, acknowledging the potential presence of surface contamination despite careful chamber preparation procedures. To address this limitation and enhance data quality, NEXAFS data was collected after mechanically polishing the films to remove surface contaminants. Both XPS and NEXAFS measurements were performed at beamline no. 12 of the SAGA Light Source with the approval of the Kyushu Synchrotron Light Research Centre. The C 1 s peak in the XPS spectra was deconvoluted using a specific function (Voigt function, GL30) after background subtraction using a well-established method (Shirley's method) within specialized software (CasaXPS software, version 2.3.18PR1.0). This deconvolution process allowed for the identification of different chemical bonding environments within the film. Additionally, X-ray wide-range scanning with a monochromatic light source (Mg Kα line, energy of 1253.6 eV) was used to determine the elemental composition of the film surface.

Raman spectroscopy was employed to delve deeper into the structural properties of the films, particularly the abundance of C sp^3 bonds observed by XPS and the presence of the strong σ* resonance. A Lambda Vision Raman spectroscopic system (MicroRAM-300ATG) equipped with advanced components like a confocal microscope and a high-performance cooled CCD detector was used for this analysis. The samples were illuminated with a 532 nm laser beam at a low power (≤ 1.5 mW with a 5 % filter) to minimize potential damage. The laser spot size was approximately 1 μm, allowing for focused analysis. The acquisition time was 5 minutes per sample.

For direct comparison with the NDC film, the Raman spectrum of the CVD diamond film was also collected. However, to account for the potentially different phases present in the CVD diamond film (diamond grains and amorphous carbon matrix), a larger area (20 ×20 μm^2) was analysed. To ensure accurate interpretation of the Raman spectra, the wavenumber axis was calibrated using a standard crystalline Si sample with its characteristic peak at 520.6 cm^{-1}. Additionally, a single crystalline diamond (SCD) sample, known to contain 100 % C sp^3 bonds, was also analysed as a reference. As expected, the SCD exhibited a single peak at a wavenumber of 1332 cm^{-1}. Finally, the acquired Raman spectra were subjected to fitting and deconvolution using Gaussian functions. This process allowed for the separation of the overall spectrum into individual component peaks, providing a more detailed understanding of the vibrational modes within the films.

3. Results and discussion

3.1. Growth of NDC films

A comparison of the growth and preparation conditions for the studied films (NDC, ta-C, and CVD diamond) deposited on WC−Co substrates is presented in Table 1. Notably, the NDC film was fabricated using the CAPD technique on WC−Co substrates without any external heating applied to the substrate. In contrast, ta-C film deposition employed the arc ion plating method at a substrate temperature (T_s) of approximately 150 °C, while CVD diamond film fabrication utilized the hot-filament chemical vapor deposition (HF-CVD) method at a significantly higher T_s of around 800 °C. Additionally, unlike CVD diamond films, the deposition process for NDC films does not require chemical etching of Co atoms or the pre-seeding of nanodiamonds on the substrate surface. This eliminates additional processing steps and potentially reduces fabrication complexity.

The NDC film can grow with the highest deposition rate of 3.5 μm/h which is larger with 7 factors compared with that of ta-C and CVD diamond films. While the ta-C films tend to delaminate in case of increasing the film thickness larger than 0.5 μm, the NDC film has a significantly larger thickness of 10 μm, which is approximately 20 times thicker than ta-C films. In prior literature, it was reported that ta-C films with hardness of 58.5 GPa requires a metallic interlayer such as Cr to protect the film of 0.5 μm thickness from delamination [8]. This highlights the remarkable growth of NDC relative to ta-C at significant thicknesses without the need for an interlayer.

XPS analysis, as depicted in Fig. 1, revealed the elemental composition of the films alongside a reference spectrum of Highly Oriented Pyrolytic Graphite (HOPG). The spectra of NDC, ta-C, and CVD diamond films, along with HOPG, all exhibited C1s and O1s peaks. Carbon (C1s) is believed to be the dominant element within the films. The presence of the additional O1s peak can be attributed to ambient air exposure, a known factor influencing the properties of carbon films [37]. Notably, the HOPG spectrum displays a minimal O1s peak, suggesting negligible oxidation due to its short air exposure during sample preparation. This observation supports the conclusion that the O1s peak observed in the other films likely originates from air exposure.

SEM was employed to characterize the film thickness and surface morphology of the NDC film, as shown in Fig. 2. The micrograph reveals a dense film structure with fine, columnar growth, consistent with features typically observed in cathodic arc deposition processes. Notably, the film exhibits a homogenous growth across the WC−Co substrate surface, characterized by a fine clustering pattern resembling a cauliflower-like morphology. The impressive film thickness of 10 μm and the observed columnar growth can be attributed to several contributing factors [38]. Highly energetic particles ejected from the CAPD anode bombard the substrate, promoting film growth. Additionally, the inherent surface roughness of the WC−Co substrate provides a greater number of nucleation sites for film initiation with lower internal stress and enhanced adhesion strength. Finally, the close

Table 1
Comparison in growth and mechanical properties of NDC, ta-C, and CVD diamond films.

Parameters & materials	ta-C	NDC	CVD diamond
Deposition technique	Arc ion plating	CAPD	HF-CVD
Substrate temperature (°C)	~150	Room Temp. (RT)	700–800
Substrate pre-treatment	polishing	roughening	roughening + etching ofCo + seeding
Deposition rate (μm/h)	0.5	3.5	0.5
Film thickness (μm)	0. 5	10	10

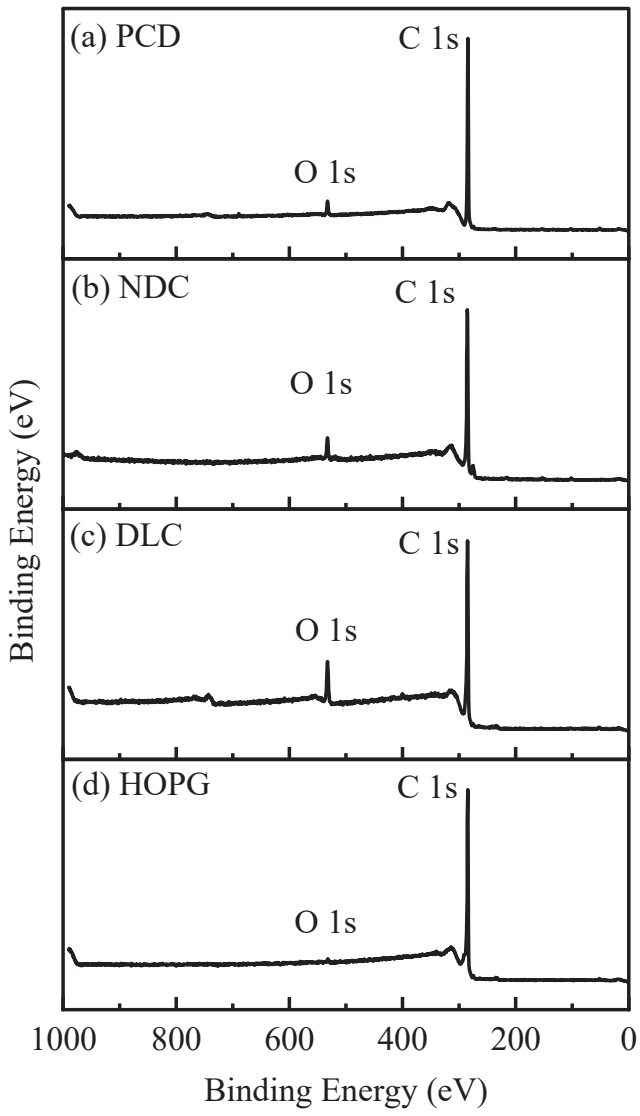

Fig. 1. X-ray survey of NDC, DLC, and PCD films along with HOPG.

target-to-substrate distance of 10 mm enhances the deposition rate. The achieved film thickness of 10 μm is comparable to that of the CVD diamond film used in this study. This thickness can be further increased by extending the deposition time within the CAPD process, optimizing target energy and target-substrate distance.

Furthermore, the successful deposition of thick, hard, and dense carbon films without peeling off like that occurred in ta-C films, is subject to the impact of internal stress within the films and interactions occurring at the film-substrate interface. On the contrary, when internal stress reaches high levels and Co atoms on the WC−Co substrate catalytically affect the films, an adverse effect is observed. This results in the degradation of hardness and delamination of the film, primarily caused by the conversion of sp^3 bonds to sp^2 bonds, leading to the graphitization of the films specially at the interface [21,39]. Fig. 3(a) illustrates the bending deflection curve of a 175 nm thick NDC film deposited on a Si (100) substrate. The curvature of this deflection profile provides valuable insights into the internal stress state within the film. In this instance, the observed convex shape is indicative of compressive internal stress within the film. Utilizing Stoney's formula, specifically the variant applicable to long and narrow samples, the internal stress (σ) of the film was estimated to be approximately 2.77 GPa [23,40].

$$\sigma = \frac{E_s}{3(1-\nu_s)} \frac{t_s^2 \delta}{I^2 t_f}$$

In this context, Es, t_s, and ν_s represent the Young's modulus, thickness, and Poisson's ratio of the silicon (Si) substrate, respectively. For the film itself, δ, I, and t_f denote the bending deflection, distance from the neutral axis to the film center, and film thickness, respectively. The value of δ, crucial for calculating the curvature, is determined by measuring the film's deflection profile as depicted in Fig. 3(a)

Fig. 3(b) provides a comparison of hardness, film thickness, and compressive stress between literature findings of DLC, and diamond films summarised in Fig. 3(c), and the newly developed NDC films. The compressive internal stress in the NDC film (2.77 GPa) is relatively low compared to other DLC films that exhibit hardness values exceeding 40 GPa. The hardest DLC films, known as ta-C, have a remarkable hardness of 85 GPa. These films suffer from a compressive stress of approximately 9.3 GPa, which is three times higher than the value in NDC films. According to Yin et al., ta-C films generally exhibit compressive stress levels ranging from 5 to 16 GPa [41]. Researchers have proposed that this high residual stress arises due to the formation of C–C sp^3 bonds during the initial growth phase of the film [32,42]. In addition, the CVD diamond film, which was analysed alongside the NDC film and shares a similar thickness of 10 μm, demonstrates a compressive stress of 4.33 GPa.

The ability to deposit thicker films without delamination can be primarily attributed to the low compressive internal stress within the NDC films. This observation suggests that the presence of a high density of grain boundaries (GBs) within the film structure plays a crucial role in effectively mitigating internal stress buildup. Nanodiamond grains are known to possess a significant number of GBs, acting as interfaces

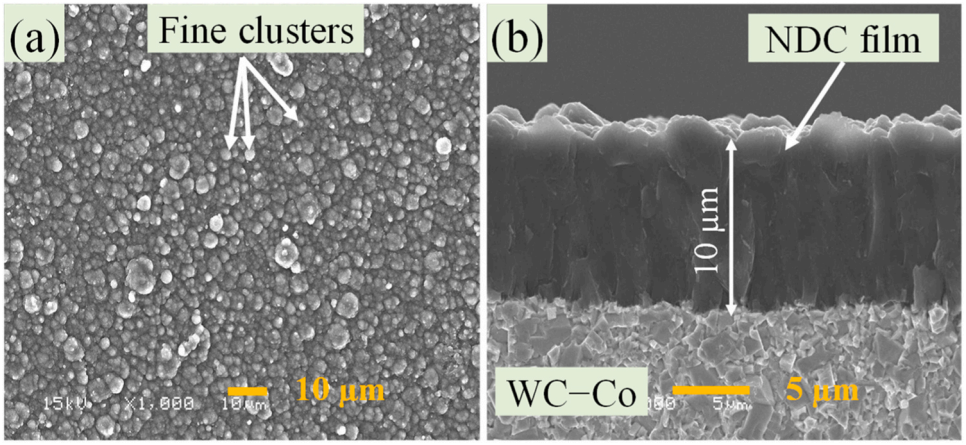

Fig. 2. (a) top view and (b) cross-sectional SEM image of NDC films.

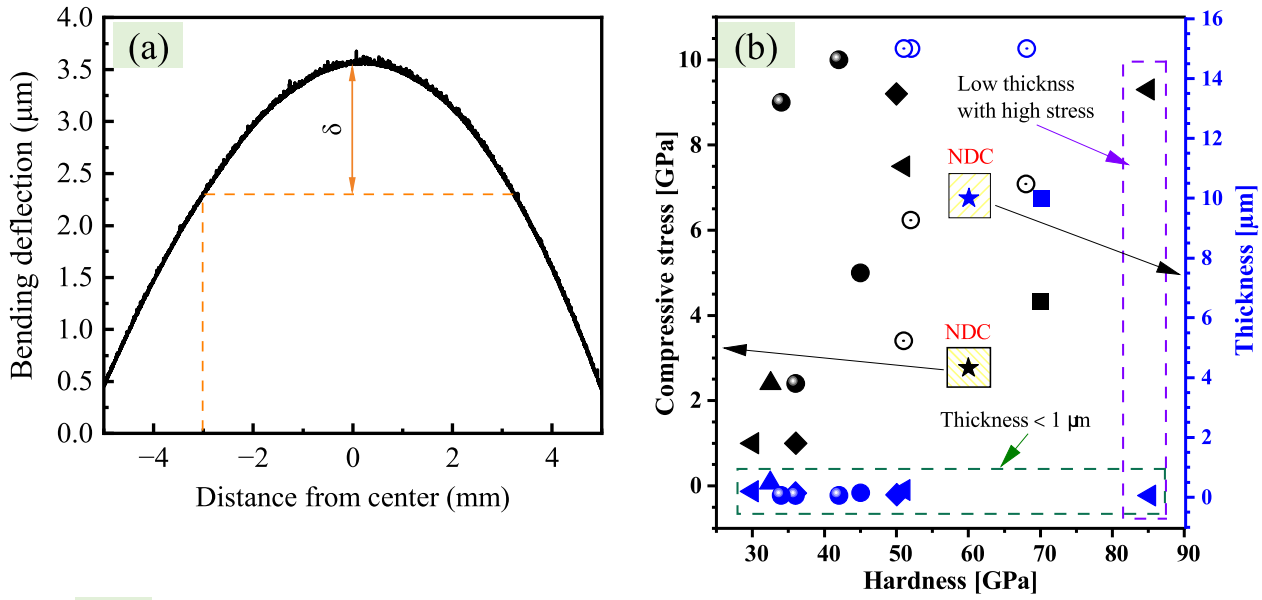

(c)

Stress	Thickness	Films materials & ref.
◀	◀	**ta-C**, Y.B. Zhang et al., Sur. & Coa. Tech., 195 (2005) 338.
●	●	**DLC**, H.J.Scheibe et al., Thin Solid Films, 246 (1994) 92.
▲	▲	**DLC**, W.Zhang et al., Diam. & rel. Mat., 11 (2002) 1837.
◆	◆	**DLC**, D.Sheeja et al., Wear, 249 (2001) 433.
★	★	**NDC**, (our film).
●	●	**ta-C**, Shi Xu et al ., Journal of Applied Physics 79, 7234 (1996).
⊙	⊙	**BBD**, M. Lu et al.,Journal of Manufacturing Processes 88 (2023) 145–156.
■	■	**CVD diamond**, (our film).

Fig. 3. (a) Bending deflection curve of NDC film with thickness of 175 nm deposited on 260-μm Si (100) substrate measured by surface roughness meter, (b) comparison among film thickness, compressive stress, and hardness of NDC, DLC, and CVD diamond films.

between individual nanodiamond grains and between the nanodiamond grains and the surrounding amorphous carbon (a-C) matrix [43,44]. This characteristic further supports the notion that the NDC film structure consists of nanodiamond grains embedded within an a-C matrix, inherently containing numerous GBs. These GBs likely act as effective pathways for stress relaxation within the film, contributing to its enhanced resistance against delamination during the deposition of thicker coatings.

3.2. *Mechanical properties of NDC films*

Nanoindentation testing revealed that NDC films possess a desirable combination of high hardness and uniformity. Notably, these NDC films boast an impressive average hardness of around 65 GPa, which is the same hardness measured for ta-C films investigated within this study. This finding positions NDC as a potential alternative material for ta-C in cutting tools coatings. Fig. 4 presents representative load-unload curves obtained from multiple locations on the film surface. These curves, encompassing the loading, holding, and unloading phases, demonstrate a consistent distribution of hardness across the film. Notably, the as-deposited film surface required polishing from its initial roughness (Ra= 0.159 μm), which matched the roughness of the WC−Co substrate Ra = 0.15–0.25 μm), to a near-mirror finish (Ra ≤ 20 nm) for accurate hardness measurements. This polishing step adheres to standard nanoindentation protocols to eliminate the influence of surface irregularities on the measured hardness values.

The tribological performance of the NDC films, as illustrated in Fig. 5, further underscores their potential for practical applications. While the as-deposited NDC film exhibited a high initial coefficient of friction (COF), this value remained lower compared to that of CVD diamond. A key advantage lies in the stability of the COF. Unlike the ta-C films, which completely delaminated after a few seconds under friction testing, or the CVD diamond coating, which displayed an unstable and continuously increasing COF over time, the NDC films maintained a remarkably stable and low COF (≤ 0.1) throughout the entire 60-minute test duration. This stable low COF translates to a significant reduction in the substrate's surface COF (from > 0.25 to ≤ 0.1). These findings highlight the competitive potential of NDC films as hard coatings, offering superior tribological performance compared to established options like ta-C and CVD diamond.

The tribological behavior of DLC films is highly sensitive to both intrinsic (chemical and structural properties) and extrinsic (testing environment) factors [45]. This wide range of observed COFs (0.001–0.7) highlights this sensitivity compared to other materials [46]. The harsh conditions including high speed, heavy load, and rough counter faces, like the Al_2O_3 disk Ra = 355 nm) used here, can significantly increase friction and wear due to interlocking asperities, especially during initial sliding stages (Fig. 5**a**). Consequently, the thin ta-C film delaminated within 5 seconds under these harsh conditions. Conversely, ta-C films exhibited a low and stable COF (0.06) under less demanding test conditions, demonstrating the dependence of tribological performance on these factors.

To evaluate the practical application potential of NDC films as competitive hard coatings compared to CVD diamond films, adhesion tests were conducted through Rockwell testing at 60 and 100 Kg, as depicted in Fig. 6. Rockwell indentation is a well-established industry

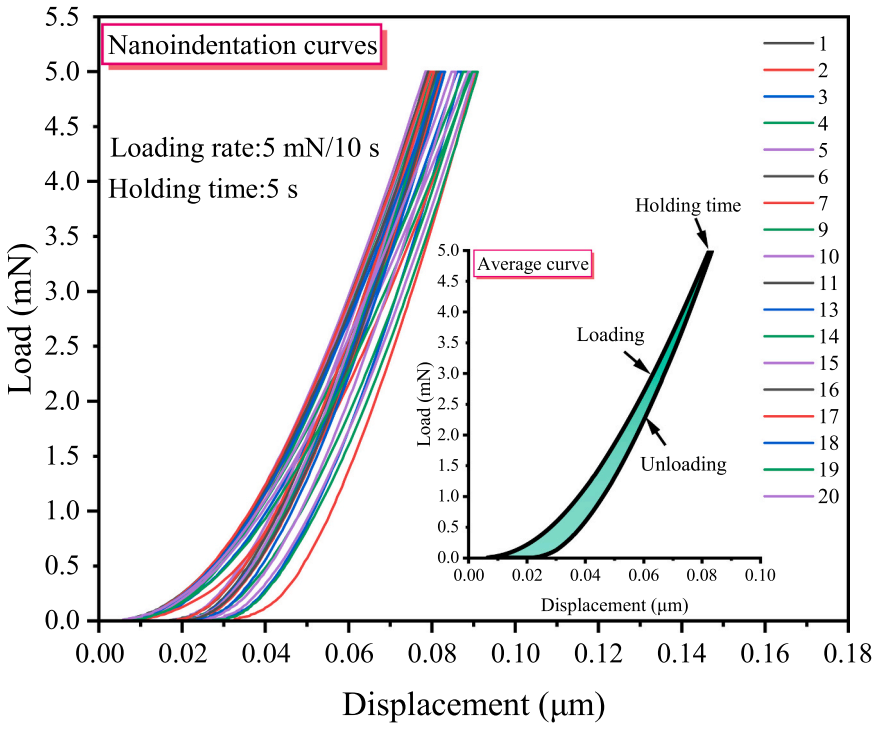

Fig. 4. Nanoindentation curves of NDC film at 20 point and their average curve.

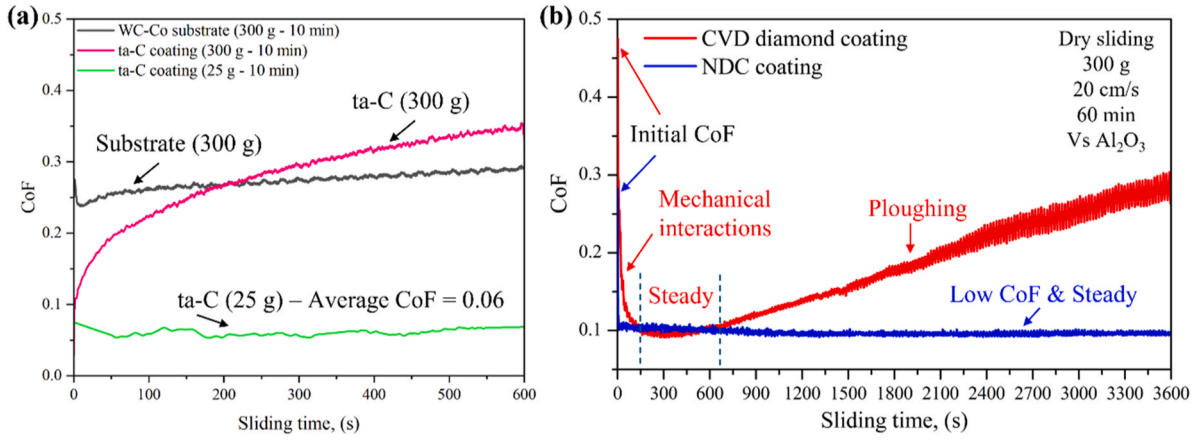

Fig. 5. Friction curves for (a) WC–Co and ta-C under loads of 25 and 300 N for 10 minutes, and (b) NDC and CVD diamond films against Al_2O_3 for 60 minutes.

method for assessing the adhesion quality of hard coatings and offers a cost-effective alternative to complex and expensive nano-indentation equipment [47]. Fig. 6(a and b) reveals the results for NDC films, where minimal or no spallation in the failure image indicates satisfactory adhesion, suggesting that NDC films exhibit acceptable adhesion strength. In contrast, Fig. 5(c and d) presents the outcomes for CVD microcrystalline diamond films, demonstrating buckling at an initial debonding load of 60 Kg, followed by delamination at 100 Kg, indicating poor adhesion. Fig. 6(e and f) exhibits more significant buckling radius and excessive delamination in CVD nanocrystalline diamond. The higher compressive stresses in the CVD microcrystalline diamond film (4.5 GPa) compared to NDC films (2.77 GPa) likely contribute to the improved adhesion of NDC films. Additionally, factors such as the nanostructured composition and the deposition of NDC films without external substrate heating may contribute to enhancing the adhesion of NDC films.

3.3. X-ray photoelectron spectroscopy (XPS) analysis

To understand the physical factors contributing to the high hardness of NDC films (65 GPa), the fraction of C sp^3 bonding was estimated and compared with that of a ta-C film with a similar hardness. XPS investigation was performed on both films using a synchrotron radiation (SR) source at an energy of 350 eV. Fig. 7 displays the obtained C1s spectra, which were analysed to identify four distinct peaks. Accurate determination of the chemical bonding state from XPS spectra relies on the peak position and shape, which are crucial parameters. The peaks observed in the C 1 s spectra were assigned based on established binding energies reported in literature [48]. These included: C═C (sp^2) at 284.53 eV, C–C (sp^3) at 285.1 eV, C–O/C–O–C at 286.63 eV, and C═O/COOH at 288.53 eV. Notably, the energy difference between the C sp^3 and C sp^2 peaks was maintained at the expected value of 0.57 eV.

The presence of a tailing effect observed in the spectra suggested surface sensitivity to oxygen and hydrogen adsorption during and after film deposition [37]. This tail likely originated from C–O/C–O–C and

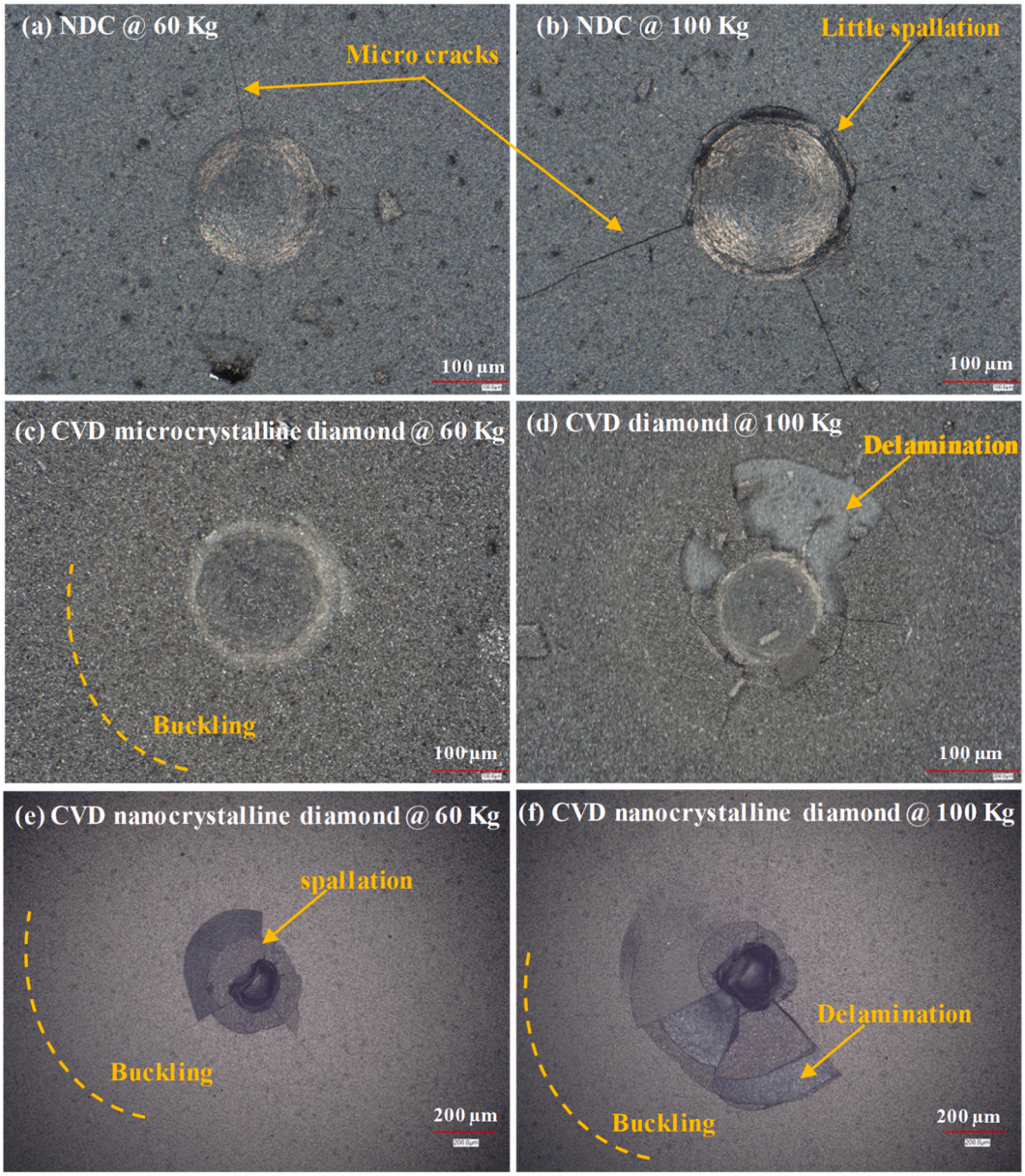

Fig. 6. Rockwell testing of (a and b) NDC film, (c and d) CVD nanocrystalline diamond film, and CVD microcrystalline diamond film on WC–Co at 60 and 100 kg loads.

C═O/COOH bonds. To minimize this effect and enhance data quality, the samples were stored in a vacuum desiccator containing silica gel, which effectively absorbed oxygen and hydrogen atoms.

The analysis revealed a sp^3 bonding fraction of approximately 70 % relative to the total carbon bonding (sp^3 + sp^2) for both films. This finding aligns well with their comparable hardness values of 65 GPa. The XPS results suggest that the high proportion of sp^3 bonds, similar to what is observed in ta-C films, plays a significant role in the hardness of the NDC film. To gain further insights into the bonding configuration, NEXAFS and Raman spectroscopy were employed for further characterization.

3.4. NEXAFS spectroscopy

NEXAFS spectroscopy was employed to gain a deeper understanding of the electronic bonding configurations within the films. The spectra of NDC films, ta-C, and CVD diamond were compared to a reference material (HOPG) for accurate interpretation. The analysis involved fitting the spectra using Gaussian functions with an error function step at 330 eV, as shown in Fig. 8 [15]. The red line in the figure represents the integral spectrum reconstructed from the decomposed components.

A key observation was the distinct difference in the spectra between 285 eV and 290 eV, indicating the presence of multiple overlapping peaks within this region. The absorption band corresponding to the C 1 s →π* disordered transition, indicative of sp^2 bonding, was further deconvoluted into two component peaks: π* C═C at 284.95 eV and π* C≡C at 287.27 eV [49]. Additionally, a surface-sensitive π* C═O peak was identified at 286.5 eV [15,50].

The absorption bands arising from the C 1 s →σ* transitions, spanning the energy range of 288 eV to 320 eV, were further decomposed into σ* C–C at 288.54 eV, σ* C═C at 293 eV, and σ* C≡C at 300 eV [49,51]. Notably, the high intensity of the σ* C–C peak in the NDC film spectra suggests a larger fraction of sp^3 bonds, similar to ta-C films. This observation aligns with the presence of nanodiamond grains within the NDC film, which contribute to the enhanced σ* C–C bonding and potentially stabilize the electronic states.

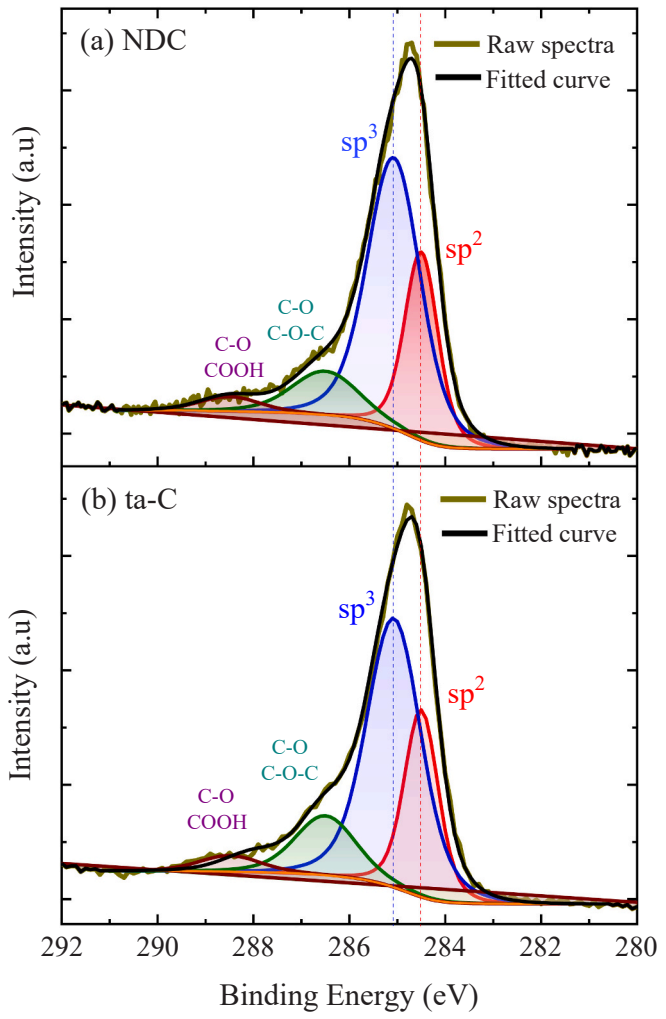

Fig. 7. C 1 s XPS spectra of the (a) NDC and (b) ta-C films.

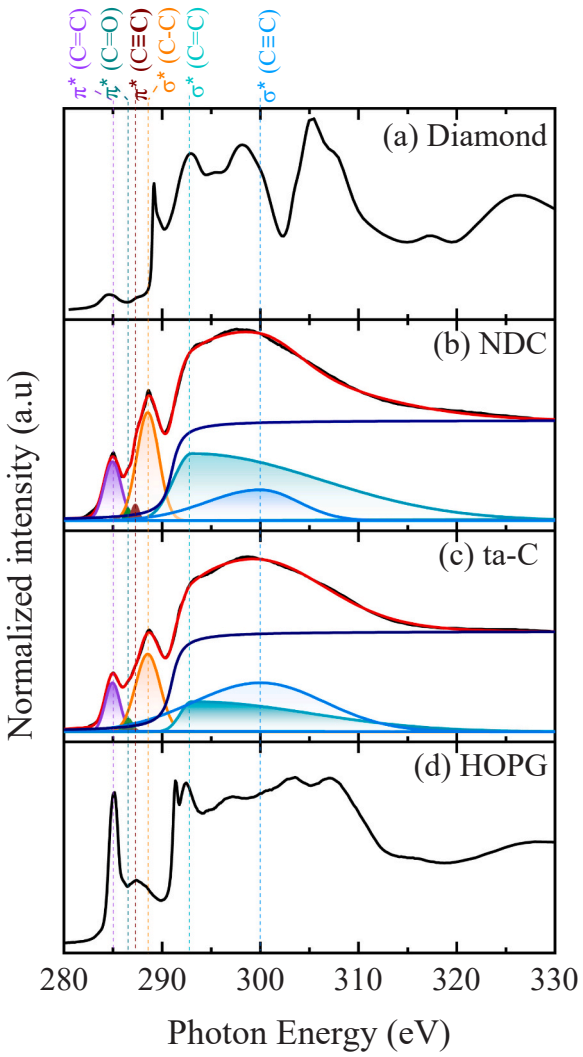

Fig. 8. Decomposed C K-edge NEXAFS spectra acquired in TEY mode of NDC and ta-C films along with spectra of CVD diamond and HOPG for comparison.

Furthermore, the NEXAFS analysis revealed a higher concentration of σ* C═C bonds in the NDC film compared to ta-C. This characteristic is believed to contribute to the increased hardness of NDC films by promoting sp^3 bonding. However, the NDC film also exhibits a greater abundance of both π* C═C and π* C≡C bonds, which are associated with sp^2 bonding. The presence of nanodiamond grains likely leads to a higher number of grain boundaries within the NDC film, potentially explaining the increased concentration of these sp^2-related bonds [52]. Interestingly, the significant presence of π* C≡C bonds in the NDC film is thought to play a crucial role in maintaining structural integrity and preventing degradation.

Conversely, the ta-C film exhibits a higher amount of σ* C≡C bonding, which also contributes to the sp^3 bonding fraction. The linear structure of σ* C≡C bonds promote stronger interatomic bonds, leading to increased film hardness and improved mechanical strength. This suggests that a balance between the total sp^3 fraction in the two films may be achieved, as indicated by XPS findings.

The presence of different types of bonding, including σ* C–C, σ* C═C, and π* C≡C, influences the mechanical and structural properties of the films. The higher concentration of sp^3 bonding and σ* C═C bonds contribute to enhance hardness of NDC film, while the presence of π*C═C and π* C≡C bonds help maintain its structural integrity and release the compressive stress due to forming high number of GBs. The ta-C film, with its higher portion of σ* C≡C bonding, also exhibits improved hardness and mechanical strength despite the NDC film has much more C–C sp^3 bonding with similar sp^3 fraction.

3.5. *Visible Raman analysis*

Raman spectroscopy is a well-established analytical technique widely employed for the characterization of thin films. It offers valuable insights into various film properties, including crystallite size, structural perfection, internal stress, and the presence of sp^3 and sp^2 carbon phases. By analysing the peak broadening and shifts observed in the Raman spectra, detailed information about the structural characteristics of CVD diamond, NDC, and ta-C films can be extracted. Therefore, the acquired Raman spectra of each film were deconvoluted into individual component peaks using Gaussian functions, as illustrated in Fig. 9. This deconvolution process allows for a more precise understanding of the subtle spectral features associated with each film type and their underlying structural configurations.

The deconvoluted Raman spectra of the films revealed the presence of several component bands, including the t-PA_1 and t-PA_2 peaks. The t-PA_1 peak was observed at approximately 1140 cm^{-1} in both NDC and CVD nanocrystalline diamond films. The t-PA_2 peak exhibited slight variations in its position across the different film types, appearing at 1496 cm^{-1} in NDC, 1465 cm^{-1} in CVD nanocrystalline diamond, and 1490 cm^{-1} in CVD microcrystalline diamond film. Existing literature suggests that the typical range for the t-PA_1 peak lies between 860 and 1170 cm^{-1}, while the t-PA_2 peak typically falls within the 1430–1496 cm^{-1} range [53–57]. The presence of both these peaks in the

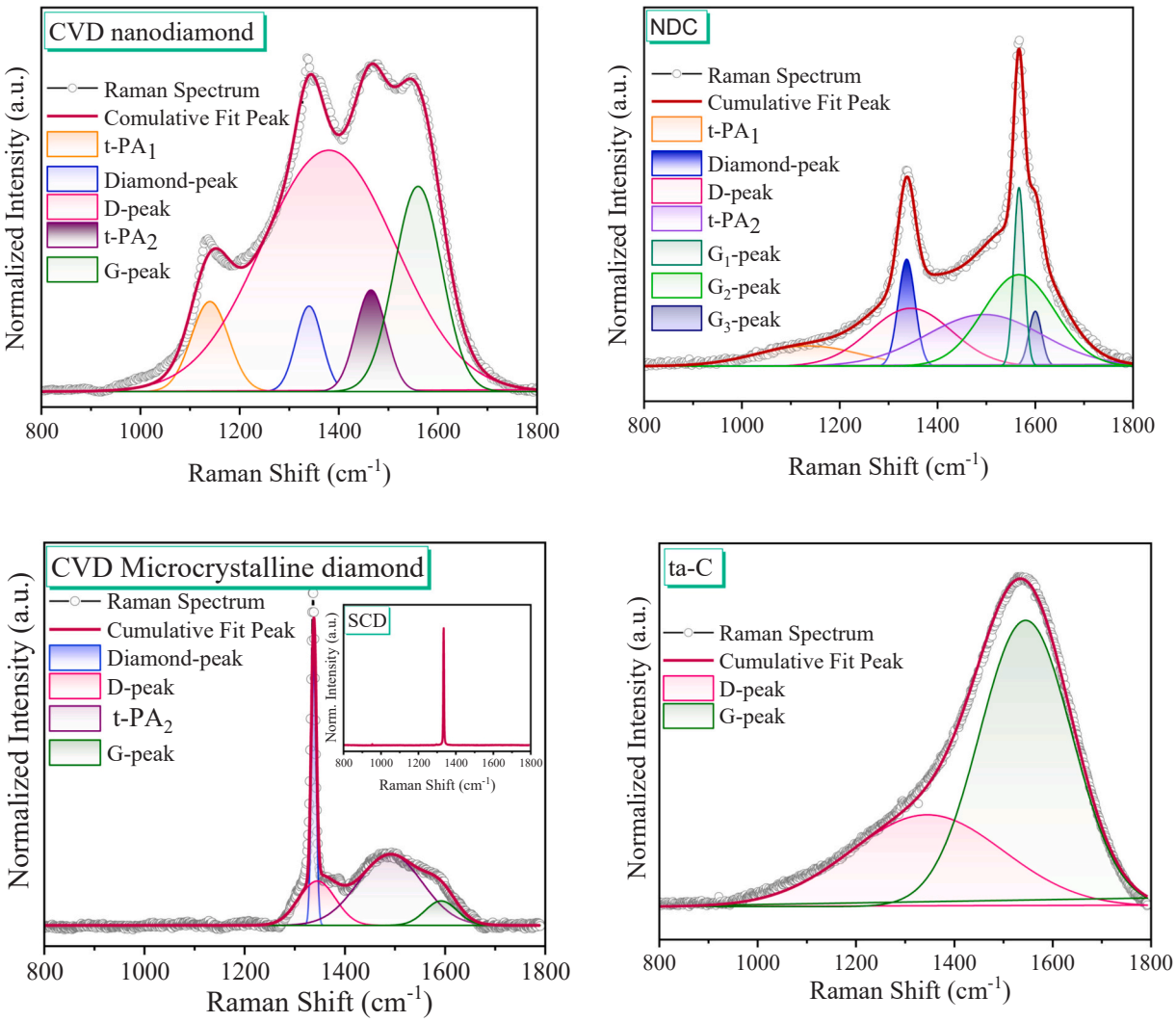

Fig. 9. Decomposed Raman spectra of CVD nanocrystalline diamond, CVD microcrystalline diamond, NDC, and DLC films along with spectrum of single crystal diamond (SCD) for comparison (onset).

Raman spectra of NDC films, along with CVD nanocrystalline diamond films, indicates a diamond phase with a nanocrystalline structure, encompassing both nanocrystalline and ultrananocrystalline diamond domains [58]. Interestingly, an inverse relationship was observed between the intensities of the t-PA_1 and t-PA_2 peaks. This phenomenon is evident in the CVD microcrystalline diamond film, where a significant increase in the t-PA_2 peak intensity is accompanied by a diminished t-PA_1 peak.

The observed t-PA_1 and t-PA_2 peaks in the Raman spectra are attributed to the presence of trans-polyacetylene segments (t-PA) within the films, consisting primarily of sp^2 hybridized carbon atoms. These segments are predominantly located at the grain boundaries (GBs) within the film structure [53]. The specific components of these peaks arise from different arrangements of C═C stretching and C−H wagging modes within the t-PA chains, where sp^2 hybridized carbon atoms alternate between bonding with one hydrogen atom and one carbon atom. The presence of these peaks confirms the existence of a high density of GBs within the NDC films. These GBs are believed to play a crucial role in relieving the internal compressive stress within the film. This stress mitigation mechanism, facilitated by the presence of numerous GBs, allows for the growth of NDC films with thicknesses comparable to those achieved with CVD diamond deposition techniques.

Generally, the peak observed at 1332 cm^{-1} corresponds to the first-order Raman diamond peak, which provides clear evidence of the presence of diamond phase characterized by C−C sp^3 bonding, as shown in the reference sample of single crystal diamond (SCD). It was reported that, Raman peaks can undergo frequency shifts, either higher or lower, due to a range of factors. These include effects from laser-induced heating and the presence of defects, disorder, and impurities in the structural arrangement [59]. Furthermore, broadening and shifting of the diamond peak likely result from reduced confinement length due to nanodiamond phonon and internal stress within the films [60,61]. The compressive stress causes the peak shifts towards higher wavenumbers, while tension stress causes the peak to shift towards lower wavenumbers, which can be evaluated using the following equation [62]:

$$\sigma = -0.567\ (\nu - \nu_0)$$

Where σ is the internal stress in GPa, ν is the wavenumber of the measured diamond peak, and $\nu_0 = 1332\ cm^{-1}$ of the standard stress-free diamond [63]. In the case of the CVD nanocrystalline diamond film, the diamond peak is located at 1339 cm^{-1}, indicating a compressive internal stress of 3.969 GPa aligned with previously reported findings of nanocrystalline diamond [64]. Additionally, CVD microcrystalline diamond displayed a notably intense diamond peak at 1338 cm^{-1}, indicative of compressive internal stress measuring 3.4 GPa. On the other hand, the NDC film exhibits a diamond peak at a wavenumber of 1337 cm^{-1} [65], indicating a lower compressive stress of 2.835 GPa. The calculated internal stresses, based on the Raman shifting of the

diamond peaks, align with those obtained from curvature method (2.77 GPa) and XRD (4.33 GPa) methods for NDC and CVD microcrystalline diamond films, respectively. This consistency confirms that the internal stress within the NDC films is lower compared to that of the CVD diamond film, as well as hard DLC (5−16 GPa). Additionally, the presence of t-PA peaks indicates the existence of GBs due to the formation of nanodiamond phase, which plays a role in suppressing internal stress in the NDC films.

The D-peak in the Raman spectrum of the NDC film was observed at 1345 cm^{-1} as well as in the CVD microcrystalline diamond and ta-C films. while in the CVD nanocrystalline diamond film, it was observed at 1380 cm^{-1}. This peak has been assigned in carbon allotropes between 1300 and 1380 cm^{-1} [66]. It is indicative of disordered or defective carbon structures within the amorphous matrix of the films. It arises from the breathing modes of sp^2 carbon rings with dangling bonds. Notably, in the visible Raman spectra, the diamond peak is overlapped with the D-peak in both NDC and CVD diamond films [67]. This overlap occurs owing to disordered A1g breathing modes of sp^2 hybridized carbon in rings, reflects the presence of amorphous/graphitic carbons at grain boundaries. The grain boundaries present in NDC films can serve as impediments to dislocation movement, hindering the propagation of defects and thereby enhancing the mechanical strength. This observation aligns with the results obtained from Rockwell testing, indicating improved mechanical strength in NDC compared to CVD microcrystalline diamond films.

Raman spectroscopy, while adept at detecting graphitic carbon in diamond films, faces challenges in precisely distinguishing diamond from other carbon types [68]. This difficulty arises due to variations in Raman intensity and the presence of sp^2-bonded carbon at grain boundaries. The intensity and position of a specific peak, the D-peak, are further influenced by factors like film surface condition, the quality of the diamond film itself, and even the parameters used during Raman analysis [66,69].

In the case of the NDC film, the D-peak is positioned at a lower wavenumber (1345 cm^{-1}) compared to the studied CVD nanocrystalline diamond film (1380 cm^{-1}). This shift towards a lower wavenumber suggests a higher proportion of sp^3 hybridized carbon atoms within the NDC film, potentially due to the presence of smaller nanodiamond grains [70]. These nanodiamonds may influence the carbon bonding structure, potentially reducing disorder or defects, and leading to a modified D-peak position. Additionally, they might act as nucleation sites for ordered carbon structures, further affecting the D-peak intensity and position. Additionally, the ta-C film exhibits a D-peak at the same wavenumber (1345 cm^{-1}) as the NDC film, suggesting a substantial sp^3 fraction in both films, which aligns with the observations from XPS analysis.

The NDC films exhibit asymmetric G-peak, and thus fitted here with three components centred at 1566 cm^{-1} (G_1-peak & G_2-peak), and 1600 cm^{-1} (G_3-peak), while the CVD nanocrystalline diamond, CVD microcrystalline diamond, and ta-C films exhibited symmetric G-peaks at wavenumber of 1560 cm^{-1}, 1591 cm^{-1}, and 1545 cm^{-1}, respectively. It was reported that, the G-peak locates between 1510 and 1580 cm^{-1} and can be extended to locate around 1600 cm^{-1} in case of formation of high fraction of sp^3 chains [71,72]. This peak corresponds to the in-plane stretching vibrational mode (E2g) of carbon atoms in the hexagonal lattice structure in both ring and chain [53]. The peak position shifts to lower wavenumbers as bond disorder increases but shifts higher when the formation of sp^3 chains occurs [69]. Therefore, the existence of G_3-peak at higher wavenumber (1600 cm^{-1}) in NDC films confirm the conversion of ring sp^2 to chain sp^3 bonds, thereby enabling the formation of small carbon clusters as shown in SEM image. This implies that the matrix of NDC film contains sp^3 chains contributes to improved films hardness.

In Raman analysis, the ratio of intensity between the disorder-induced D-peak (I_D) and the G-peak (I_G) signifies the degree of structural disorder in DLC films. Similarly, the ratio of the area of the D-peak (A_D) to that of the G-peak (A_G) provides insight into the level of disordered structure in these films [56]. For the ta-C film, Raman spectroscopy reveals minimal disorder in sp^2-hybridized carbon and an enhanced graphite phase, as evidenced by the low I_D/I_G and A_D/A_G ratios. This observation indicates an I_D/I_G ratio of 0.28 % and an area ratio of 34 % for the ta-C film, indirectly suggesting a high sp^3 fraction. These ratios are consistent with XPS results ($sp^2 = 30$ %).

Raman analysis reveals that NDC films share characteristic peaks with CVD nanocrystalline diamond, including t-PA_1, t-PA_2, and diamond peaks. The improved hardness of NDC films results from the presence of nanodiamond grains and inherent features within the amorphous carbon matrix, encompassing ring and chain graphite phases. In contrast, the studied ta-C film's heightened hardness arises from a higher proportion of ring graphite phases and a decrease in disordered phases. The level of disordered phase in sp^2-hybridized carbon corresponds with measurements from NEXAFS analysis, indicated by a lower π^* resonance. Furthermore, the presence of grain boundaries in NDC films effectively supresses internal stress, contributing to the films' ability to attain considerable thickness during growth, which is a characteristic that distinguishes NDC from ta-C film.

4. Conclusion

This study successfully employed the CAPD technique to deposit thick NDC films (10 μm) on unheated WC−Co substrates, achieving a thickness of 10 μm comparable to CVD diamond films with 7 factor improved deposition rate (3.5 μm/h). The NDC films exhibited a hardness of 65 GPa, similar to ta-C films. Additionally, the NDC films significantly improved the tribological behaviour of the WC−Co substrate. Dry friction testing reduced the COF from ≥ 0.25 to a stable and low COF of ≤ 0.1 over 60 minutes. This stability contrasts with the ta-C films, which delaminated after a few seconds, and the CVD diamond coating, which showed an unstable, progressively increasing COF. A comprehensive analysis involving nanoindentation, Rockwell, SEM, XPS, NEXAFS, and Raman techniques provided valuable insights into the factors influencing the deposition of adherent NDC films with high hardness and thickness, positioning them as competitors to ta-C and CVD diamond coatings. The presence of numerous grain boundaries contributed to the low compressive stress (2.77 GPa) observed in the NDC films, enabling the growth of thick films comparable to CVD diamond. The Rockwell test indicated no delamination or minimal spallation in NDC films, in contrast to buckling and delamination observed in CVD diamond with increasing load from 60 to 100 Kg. Raman investigations revealed that NDC exhibited bands similar to CVD diamond, including t-PA peaks, which indicate a high amount of grain boundaries. These grain boundaries contribute to suppressing internal stress in the films and enhance sliding properties, resulting in a stable and low COF (≤ 0.1) in harsh conditions. The significant presence of NEAFS σ^* C−C bonds and a high C sp^3 fraction (70 %) in the NDC film can be attributed to the characteristics of the a-C matrix and the presence of nanodiamonds. This study demonstrated that NDC films deposited by CAPD exhibit a high deposition rate, exceptional hardness, superior tribological behaviour, and improved adhesion, making them a promising competitor to hard carbon coatings, particularly for cutting tool applications.

Author statement

This study investigates thick nanodiamond composite (NDC) hard coatings as potential substitutes for ta-C and CVD diamond coatings, which are limited by thickness and deposition rate. Using cathodic arc plasma deposition (CAPD), we deposited 10 μm thick NDC films on unheated WC-Co substrates at a deposition rate of 3.5 μm/h, comparable to CVD diamond but with superior adhesion. The NDC films exhibited a hardness of 65 GPa, similar to ta-C, and resisted delamination during Rockwell testing better than CVD diamond. Analysis revealed a unique

nanostructure with nanodiamond grains in an amorphous carbon matrix, high C-C sp^3 bonds (70 %), and low compressive stress (2.77 GPa), enabling thick film deposition without delamination. NDC coatings offer a competitive alternative due to their high hardness, thick film capability, fast deposition, strong adhesion, and eco-friendly CAPD process.

CRediT authorship contribution statement

Koki Murasawa: Writing – original draft, Visualization, Validation, Methodology. **Mohamed R. Diab:** Visualization, Methodology, Investigation. **Hoda Atta:** Methodology, Investigation. **Hiroshi Naragino:** Visualization, Methodology. **Abdelhamid El-Shaer:** Methodology, Investigation. **Tsuyoshi Yoshitake:** Writing – review & editing, Supervision, Funding acquisition. **Mohamed Egiza:** Writing – review & editing, Writing – original draft, Project administration, Formal analysis, Data curation, Conceptualization.

Declaration of Competing Interest

The authors declare that they have no known competing financial interests or personal relationships that could have appeared to influence the work reported in this paper.

Data Availability

The authors do not have permission to share data.

Acknowledgements

The corresponding author (M. Egiza) gratefully acknowledge the financial support provided by the Cultural Affairs and Missions Sector of the Egyptian Ministry of Higher Education. Additional financial contributions to this research were received from the Osawa Scientific Studies Grants Foundation, the Advanced Machining Technology & Development Association, JST A-STEP Stage II (seed development type AS2915051S), and JSPS KAKENHI Grant Nos. JP19H02436 and 21K18830. The XPS measurements were conducted at Beamline 12 of the Kyushu Synchrotron Light Research Center/Saga Light Source under Proposal Nos. 1704022S, 2009085S, and 2106055S.

References

[1] X. Wang, X. Shen, C. Zeng, F. Sun, Combined influences of tool shape and as-deposited diamond film on cutting performance of drills for CFRP machining, Surf. Coat. Technol. 347 (2018) 390–397, https://doi.org/10.1016/j.surfcoat.2018.05.024.

[2] D.H.Eckart Uhlmann, Walter Reimers, Katrin Botther, Multilayer structure dependent performance behaviour of CVD diamond thin film drilling tools during CFRP machining, Procedia CIRP 87 (2020) 6, https://doi.org/10.1016/j.procir.2020.02.089.

[3] J.-Y. Hwang, D.-G. Ahn, Effects of carbide substrate properties and diamond coating morphology on drilling performance of CFRP composite, J. Manuf. Process. 58 (2020) 1274–1284, https://doi.org/10.1016/j.jmapro.2020.09.028.

[4] K. Ramasubramanian, N. Arunachalam, M.S. Ramachandra Rao, Wear performance of nano-engineered boron doped graded layer CVD diamond coated cutting tool for machining of Al-SiC MMC, Wear 426-427 (2019) 1536–1547, https://doi.org/10.1016/j.wear.2018.12.004.

[5] K. Bobzin, High-performance coatings for cutting tools, CIRP J. Manuf. Sci. Technol. 18 (2017) 1–9, https://doi.org/10.1016/j.cirpj.2016.11.004.

[6] R. Dumpala, N. Kumar, C.R. Kumaran, S. Dash, B. Ramamoorthy, M. S. Ramachandra Rao, Adhesion characteristics of nano- and micro-crystalline diamond coatings: Raman stress mapping of the scratch tracks, Diam. Relat. Mater. 44 (2014) 71–77, https://doi.org/10.1016/j.diamond.2014.02.007.

[7] M.Y. Noordin, A.S. Noor Adila, S. Izman, D. Kurniawan, Acid pretreatment of WC-Co prior to CVD diamond coating, Adv. Mater. Res. 576 (2012) 626–629, https://doi.org/10.4028/www.scientific.net/AMR.576.626.

[8] K.-J. Feng, C.-Q. Guo, S.-S. Lin, Z.-Q. Fu, Q. Shi, Y.-F. Su, W. Wang, M.-J. Dai, Structure and properties of ta-C films prepared by vacuum cathodic arc with an unbalanced external electromagnetic field, Ceram. Int. 48 (1) (2022) 111–119, https://doi.org/10.1016/j.ceramint.2021.09.086.

[9] C.-Y. Cheng, F.C.-N. Hong, Growth of hydrogen-free diamond-like carbon films by a particle-free hollow-cathode arc ion plating system, Thin Solid Films 498 (1-2) (2006) 206–211, https://doi.org/10.1016/j.tsf.2005.07.089.

[10] A. M. Ali, T. Deckert-Gaudig, M. Egiza, V. Deckert, T. Yoshitake, Near- and far-field Raman spectroscopic studies of nanodiamond composite films deposited by coaxial arc plasma, Appl. Phys. Lett. 116 (4) (2020) 5, https://doi.org/10.1063/1.5142198.

[11] M. Egiza, A.M. Ali, M.R. Diab, N. Hemaya, K. Murasawa, T. Yoshitake, Synthesis and comprehensive synchrotron-based structural analysis of Si-doped nanodiamond composite films deposited on cemented carbide, Surf. Coat. Technol. 471 (2023), https://doi.org/10.1016/j.surfcoat.2023.129867.

[12] Y.X. Ou, H.Q. Wang, X. Ouyang, Y.Y. Zhao, Q. Zhou, C.W. Luo, Q.S. Hua, X. P. Ouyang, S. Zhang, Recent advances and strategies for high-performance coatings, Prog. Mater. Sci. 136 (2023), https://doi.org/10.1016/j.pmatsci.2023.101125.

[13] K. Hanada, T. Nishiyama, T. Yoshitake, K. Nagayama, Time-resolved observation of deposition process of ultrananocrystalline diamond/hydrogenated amorphous carbon composite films in pulsed laser deposition, J. Nanomater. 2009 (2009) 1–6, https://doi.org/10.1155/2009/901241.

[14] H. Naragino, A. Tominaga, K. Hanada, T. Yoshitake, Synthesis method for ultrananocrystalline diamond in powder employing a coaxial arc plasma gun, Appl. Phys. Express 8 (7) (2015), https://doi.org/10.7567/apex.8.075101.

[15] A.M. Ali, M. Egiza, K. Murasawa, H. Sugita, T. Deckert-Gaudig, V. Deckert, T. Yoshitake, Effects of substrate temperature and intermediate layer on adhesion, structural and mechanical properties of coaxial arc plasma deposition grown nanodiamond composite films on Si substrates, Surf. Coat. Technol. 417 (2021) 11, https://doi.org/10.1016/j.surfcoat.2021.127185.

[16] M. Egiza, M.R. Diab, A.W. Zia, K. Murasawa, N. Faisal, T. Yoshitake, Wear-resistant and adherent nanodiamond composite thin film for durable and sustainable silicon carbide mechanical seals, Wear 550-551 (2024), https://doi.org/10.1016/j.wear.2024.205394.

[17] L. Osman, A.M. Ali, A. Zkria, H. Naragino, T. Yoshitake, Adhesion of nanodiamond composite films on Ti substrates at room temperature via hybrid ion etching gun and coaxial arc plasma deposition, Appl. Phys. Express 15 (11) (2022), https://doi.org/10.35848/1882-0786/ac99b6.

[18] M.R. Diab, M. Egiza, K. Murasawa, H. Naragino, A. El-Shaer, T. Yoshitake, Eco-friendly thick and wear-resistant nanodiamond composite hard coatings deposited on WC–Co substrates, Surf. Coat. Technol. 479 (2024), https://doi.org/10.1016/j.surfcoat.2024.130517.

[19] M. Egiza, M. Ragab Diab, A.M. Ali, K. Murasawa, T. Yoshitake, Sustainable super-hard and thick nanodiamond composite film deposited on cemented carbide substrates with an interfacial Al-interlayer, Mater. Lett. 364 (2024), https://doi.org/10.1016/j.matlet.2024.136369.

[20] M. Egiza, A.M. Ali, K. Murasawa, T. Yoshitake, B-doped nanodiamond composite hard coatings deposited on cemented carbide: mechanical, structural, and tribological properties, Int. J. Refract. Met. Hard Mater. 114 (2023), https://doi.org/10.1016/j.ijrmhm.2023.106260.

[21] M. Egiza, H. Naragino, A. Tominaga, K. Murasawa, H. Gonda, M. Sakurai, T. Yoshitake, Si and Cr doping effects on growth and mechanical properties of ultrananocrystallinediamond/amorphous carbon composite films deposited on cemented carbide substrates by coaxial arc plasma deposition, Evergreen 3 (1) (2016) 32–36, https://doi.org/10.5109/1657738.

[22] M. Egiza, M. Ragab Diab, H. Atta, M.M. Abdelfatah, A. El-Shaer, T. Yoshitake, Unveiling a 72.5 GPa peak hardness in sustainable nanodiamond composite hard coatings via discharge energy control: A nanoindentation-Raman approach, Mater. Lett. 369 (2024), https://doi.org/10.1016/j.matlet.2024.136684.

[23] H. Naragino, M. Egiza, A. Tominaga, K. Murasawa, H. Gonda, M. Sakurai, T. Yoshitake, Hard coating of ultrananocrystalline diamond/nonhydrogenated amorphous carbon composite films on cemented tungsten carbide by coaxial arc plasma deposition, Appl. Phys. A 122 (8) (2016), https://doi.org/10.1007/s00339-016-0284-4.

[24] A.M. Ali, M. Egiza, K. Murasawa, Y. Fukui, H. Gonda, M. Sakurai, T. Yoshitake, Negative bias effects on deposition and mechanical properties of ultrananocrystalline diamond/amorphous carbon composite films deposited on cemented carbide substrates by coaxial arc plasma, Diam. Relat. Mater. 96 (2019) 67–73, https://doi.org/10.1016/j.diamond.2019.04.031.

[25] M.R. Diab, M. Egiza, K. Murasawa, S. Ohmagari, H. Naragino, T. Yoshitake, Revealing mechanical and structural properties of Si-doped nanodiamond composite films through applied biasing voltages on WC – Co substrates, Int. J. Refract. Met. Hard Mater. 119 (2024), https://doi.org/10.1016/j.ijrmhm.2023.106518.

[26] H. Naragino, M. Egiza, A. Tominaga, K. Murasawa, H. Gonda, M. Sakurai, T. Yoshitake, Room-temperature hard coating of ultrananocrystalline diamond/nonhydrogenated amorphous carbon composite films on tungsten carbide by coaxial arc plasma deposition, Jpn. J. Appl. Phys. 55 (3) (2016), https://doi.org/10.7567/jjap.55.030302.

[27] K. Hanada, T. Yoshida, Y. Nakagawa, T. Yoshitake, Formation of ultrananocrystalline diamond/amorphous carbon composite films in vacuum using coaxial arc plasma gun, Jpn. J. Appl. Phys. 49 (12R) (2010), https://doi.org/10.1143/jjap.49.125503.

[28] L. Wang, Y. Liu, H. Chen, M. Wang, Nanoindentation-induced deformation behaviors of tetrahedral amorphous carbon film deposited by cathodic vacuum arc with different substrate bias voltages, Appl. Surf. Sci. 576 (2022), https://doi.org/10.1016/j.apsusc.2021.151741.

[29] M. Mermoux, S. Chang, H.A. Girard, J.-C. Arnault, Raman spectroscopy study of detonation nanodiamond, Diam. Relat. Mater. 87 (2018) 248–260, https://doi.org/10.1016/j.diamond.2018.06.001.

[30] K. Artyushkova, S. Pylypenko, Application of surface analysis methods to study alignment mechanism and orientation of liquied crystals, J. Mol. Liq. 267 (2018) 452–549, https://doi.org/10.1016/j.molliq.2018.01.071.
[31] M. Haddad, O. Kurtulus, M. Mertens, K. Brühne, P. Glüche, H. Fecht, Optimization of residual stresses inside diamond thin films grown by hot filament chemical vapor deposition (HFCVD), Diam. Relat. Mater. 131 (2023), https://doi.org/10.1016/j.diamond.2022.109564.
[32] D.R. McKenzie, D. Muller, B.A. Pailthorpe, Compressive-stress-induced formation of thin-film tetrahedral amorphous carbon, Phys. Rev. Lett. 67 (6) (1991) 773–776, https://doi.org/10.1103/PhysRevLett.67.773.
[33] O.R. Monteiro, Plasma synthesis of hard materials with energetic ions, Nucl. Instrum. Methods Phys. Res. B 148 (1999) 5, https://doi.org/10.1016/S0168-583X(98)00685-5.
[34] J. Zheng, Z. Lu, S. Liu, J.C. Ding, S. Ran, J. Sun, Microstructure and tribological behavior in ta-C films prepared by laser-induced filtered cathodic vacuum arc technique: effect of charge voltage, Vacuum 219 (2024) 112745, https://doi.org/10.1016/j.vacuum.2023.112745.
[35] V. Bonu, G. Srinivas, V. Praveen Kumar, A. Joseph, C. Narayana, H.C. Barshilia, Temperature dependent erosion and Raman analyses of arc-deposited H free thick DLC coating on Cr/CrN coated plasma nitrided steel, Surf. Coat. Technol. 436 (2022) 128308, https://doi.org/10.1016/j.surfcoat.2022.128308.
[36] J. Wei, H. Li, L. Liu, P. Guo, P. Ke, A. Wang, Enhanced tribological and corrosion properties of multilayer ta-C films via alternating sp3 content, Surf. Coat. Technol. 374 (2019) 317–326, https://doi.org/10.1016/j.surfcoat.2019.05.087.
[37] M. Egiza, H. Naragino, A. Tominaga, K. Hanada, K. Kamitani, T. Sugiyama, E. Ikenaga, K. Murasawa, H. Gonda, M. Sakurai, T. Yoshitake, Effects of air exposure on hard and soft x-ray photoemission spectra of ultrananocrystalline diamond/amorphous carbon composite films, Coatings 8 (10) (2018), https://doi.org/10.3390/coatings8100359.
[38] B. Rauschenbach, J.W. Gerlach, Texture Development in Titanium Nitride Films Grown by Low-Energy Ion Assisted Deposition, 35(6-7) (2000) 675-688. https://doi.org/10.1002/1521-4079(200007)35:6/7<675::AID-CRAT675>3.0.CO;2-7.
[39] M. Egiza, K. Murasawa, A.M. Ali, Y. Fukui, H. Gonda, M. Sakurai, T. Yoshitake, Enhanced hardness of nanocarbon films deposited on cemented tungsten carbide substrates by coaxial arc plasma deposition owing to employing silicon-doped graphite targets, Jpn. J. Appl. Phys. 58 (7) (2019), https://doi.org/10.7567/1347-4065/ab289f.
[40] S. Shiri, P. Ashtijoo, A. Odeshi, Q. Yang, Evaluation of Stoney equation for determining the internal stress of DLC thin films using an optical profiler, Surf. Coat. Technol. 308 (2016) 98–100, https://doi.org/10.1016/j.surfcoat.2016.07.098.
[41] Y. Yin, D.R. McKenzie, J. Zou, A. Das, The application of the cathodic arc to plasma assisted chemical vapor deposition of carbon, J. Appl. Phys. 79 (3) (1996) 1563–1568, https://doi.org/10.1063/1.362649.
[42] J. Schwan, S. Ulrich, T. Theel, H. Roth, H. Ehrhardt, P. Becker, S.R.P. Silva, Stress-induced formation of high-density amorphous carbon thin films, J. Appl. Phys. 82 (12) (1997) 6024–6030, https://doi.org/10.1063/1.366469.
[43] O. Auciello, A.V. Sumant, Status review of the science and technology of ultrananocrystalline diamond (UNCD™) films and application to multifunctional devices, Diam. Relat. Mater. 19 (7-9) (2010) 699–718, https://doi.org/10.1016/j.diamond.2010.03.015.
[44] D. Manova, J.W. Gerlach, S. Mandl, Thin film deposition using energetic ions, Mater. (Basel) 3 (8) (2010) 4109–4141, https://doi.org/10.3390/ma14185162.
[45] A. Erdemir, C.J.Jo.P.D.A.P. Donnet, Tribology of diamond-like carbon films: recent progress and future prospects, 39(18) (2006) https://doi.org/R311.10.1088/0022-3727/39/18/R01.
[46] A. Erdemir, C.J.M.A. Donnet, m.s. series, Modern Tribology Handbook, CRC Press, Boca Raton, FL, 2001, pp. 787–825, https://doi.org/10.1201/9780849377877.
[47] F. Lyu, X. Li, C. Chen, C. Liu, C. Li, M. Jiang, X. Hu, High adhesion diamond films deposited on stainless steel by using nanocomposite films with mosaic interface as an interlayer, Appl. Surf. Sci. 528 (2020), https://doi.org/10.1016/j.apsusc.2020.146916.
[48] Y. Xue, Z. Wang, J. Wang, C. Hu, F. Xie, D. Chen, Z. He, Evidence of carboxyl modification of hydrogen-free diamond-like carbon films assisted by radio frequency plasma in vacuum, ISRN Spectrosc. 2012 (2012) 1–6, https://doi.org/10.5402/2012/963298.
[49] S. Ohmagari, T. Yoshitake, A. Nagano, S. Al-Riyami, R. Ohtani, H. Setoyama, E. Kobayashi, K. Nagayama, Near-edge X-ray absorption fine structure of ultrananocrystalline diamond/hydrogenated amorphous carbon films prepared by pulsed laser deposition, J. Nanomater. 2009 (2009) 1–5, https://doi.org/10.1155/2009/876561.
[50] S. Osswald, G. Yushin, V. Mochalin, S.O. Kucheyev, Y. Gogotsi, Control of sp2/sp3 carbon ratio and surface chemistry of nanodiamond powders by selective oxidation in air, J. Am. Chem. Soc. 128 (35) (2006) 11635–11642, https://doi.org/10.1021/ja063303n.
[51] J.G. Buijnsters, R. Gago, A. Redondo-Cubero, I. Jiménez, Hydrogen stability in hydrogenated amorphous carbon films with polymer-like and diamond-like structure, J. Appl. Phys. 112 (9) (2012), https://doi.org/10.1063/1.4764001.
[52] X. Xiao, J. Birrell, J.E. Gerbi, O. Auciello, J.A. Carlisle, Low temperature growth of ultrananocrystalline diamond, J. Appl. Phys. 96 (4) (2004) 2232–2239, https://doi.org/10.1063/1.1769609.
[53] A.C. Ferrari, J. Robertson, Origin of the1150−cm−1Raman mode in nanocrystalline diamond, Phys. Rev. B 63 (12) (2001) 121405(R), https://doi.org/10.1103/PhysRevB.63.121405.
[54] X. Song, M. Lu, H. Wang, X.C. Wang, F.H. Sun, Fracture mechanics of microcrystalline/nanocrystalline composited multilayer chemical vapor deposition self-standing diamond films, Ceram. Int. 48 (15) (2022) 21868–21878, https://doi.org/10.1016/j.ceramint.2022.04.173.
[55] J. Peng, J. Zeng, Y. Xiao, W. Li, Novel conversion annealing pretreatment for improved deposition of diamond coatings onto WC-Co cemented carbide, J. Alloy. Compd. 893 (2022), https://doi.org/10.1016/j.jallcom.2021.162325.
[56] B. Paramanik, D. Das, Synthesis of nanocrystalline diamond embedded diamond-like carbon films on untreated glass substrates at low temperature using (C2H2 + H2) gas composition in microwave plasma CVD, Appl. Surf. Sci. 579 (2022), https://doi.org/10.1016/j.apsusc.2021.152132.
[57] M.A. Philip, U. Natarajan, R. Nagarajan, Acoustically-enhanced particle dispersion in polystyrene/alumina nanocomposites, Adv. nano Res. 2 (2) (2014) 121–133, https://doi.org/10.12989/anr.2014.2.2.121.
[58] J. Birrell, J.E. Gerbi, O. Auciello, J.M. Gibson, J. Johnson, J.A. Carlisle, Interpretation of the Raman spectra of ultrananocrystalline diamond, Diam. Relat. Mater. 14 (1) (2005) 86–92, https://doi.org/10.1016/j.diamond.2004.07.012.
[59] L. Zhang, H. Li, K.-T. Yue, S.-L. Zhang, X. Wu, J. Zi, Z. Shi, Z. Gu, Effects of intense laser irradiation on Raman intensity features of carbon nanotubes, Phys. Rev. B 65 (7) (2002), https://doi.org/10.1103/PhysRevB.65.073401.
[60] S. Prawer, R.J. Nemanich, Raman spectroscopy of diamond and doped diamond, Philos. Trans. A Math. Phys. Eng. Sci. 362 (1824) (2004) 2537–2565, https://doi.org/10.1098/rsta.2004.1451.
[61] A. Roy, D. Das, Synthesis of single-walled, bamboo-shaped and Y-junction carbon nanotubes using microwave plasma CVD on low-temperature and chemically processed catalysts, J. Phys. Chem. Solids 152 (2021), https://doi.org/10.1016/j.jpcs.2021.109971.
[62] J.W. Ager 3rd, M.D. Drory, Quantitative measurement of residual biaxial stress by Raman spectroscopy in diamond grown on a Ti alloy by chemical vapor deposition, Phys. Rev. B Condens Matter 48 (4) (1993) 2601–2607, https://doi.org/10.1103/physrevb.48.2601.
[63] C.T. Kuo, C.R. Lin, H.M. Lien, Origins of the residual stress in CVD diamond films, Thin Solid Films 290-291 (1996) 254–259, https://doi.org/10.1016/s0040-6090(96)09016-5.
[64] Y.S. Li, L. Yang, Y. Tang, C. Zhang, L. Zhang, I. Onyeka, Q. Yang, R. Feng, A. Hirose, Adherent nanocrystalline diamond coatings deposited on Ti substrate at moderate temperatures, Surf. Coat. Technol. 206 (7) (2011) 1971–1976, https://doi.org/10.1016/j.surfcoat.2011.09.077.
[65] D.-D. Ma, Y.-P. Xue, J. Gao, Y. Ma, S.-W. Yu, Y.-S. Wang, C. Xue, H.-J. Hei, B. Tang, Effect of Ta diffusion layer on the adhesion properties of diamond coating on WC-Co substrate, Appl. Surf. Sci. 527 (2020), https://doi.org/10.1016/j.apsusc.2020.146727.
[66] H.-J. Wang, D.-W. Zuo, F. Xu, W.-Z. Lu, Fabrication of nano-crystalline diamond duplex micro-gear by hot filament chemical vapor deposition, Mater. Trans. 58 (1) (2017) 91–94, https://doi.org/10.2320/matertrans.M2016334.
[67] A. Dychalska, P. Popielarski, W. Franków, K. Fabisiak, K. Paprocki, M. Szybowicz, Study of CVD diamond layers with amorphous carbon admixture by Raman scattering spectroscopy, Mater. Sci. -Pol. 33 (4) (2015) 799–805, https://doi.org/10.1515/msp-2015-0067.
[68] D.W. Ren, Q. Zhao, A. Bendavid, Anti-bacterial property of Si and F doped diamond-like carbon coatings, Surf. Coat. Technol. 226 (2013) 1–6, https://doi.org/10.1016/j.surfcoat.2013.03.025.
[69] A.C. Ferrari, A.C. Ferrari, J. Robertson, J. Robertson, Raman spectroscopy of amorphous, nanostructured, diamond–like carbon, and nanodiamond, Philos. Trans. R. Soc. Lond. Ser. A: Math. Phys. Eng. Sci. 362 (1824) (2004) 2477–2512, https://doi.org/10.1098/rsta.2004.1452.
[70] D. Das, A. Banerjee, Further improvements of nano-diamond structures on unheated substrates by optimization of parameters with secondary plasma in MW-PECVD, Surf. Coat. Technol. 272 (2015) 357–365, https://doi.org/10.1016/j.surfcoat.2015.03.042.
[71] A.C. Ferrari, J. Robertson, Raman spectroscopy of amorphous, nanostructured, diamond–like carbon, and nanodiamond, Philos. Trans. R. Soc. Lond. Ser. A: Math., Phys. Eng. Sci. 362 (1824) (2004) 2477–2512, https://doi.org/10.1098/rsta.2004.1452.
[72] K. Aoki, K. Suzuki, K. Ishii, K. Takanashi, T. Komukai, K. Oura, T. Hirao, Formation of nanoscale diamond particles without substrate heating by cathodic arc deposition, Jpn. J. Appl. Phys. 44 (5L) (2005), https://doi.org/10.1143/jjap.44.L746.